significant design features are large modern windows and blue coloured metal encasements. The object has 8 floors and no lower basement. The flat roof has no lofts. Building front side faces southbound. Partial balcony miradors can be identified as sectional sunshades, but are not capable to avoid intensive overheating of the building during the hot season. Absence of any surrounding shading object and large tarmac car park escalates unpleasant situation [3].

Aerial overview of the sample object is presented on Fig. 1. Locations of particular sample rooms are highlighted in red circles.

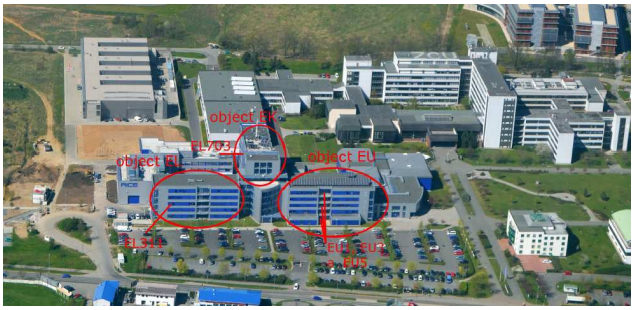

Fig. 1. Aerial view of the model object.

Five sample rooms were selected to respect the architecture, location and orientation of the building:

- 1st floor - corridor (NE – SW)
- 3rd floor – corridor (NE – SW)
- 5th floor – corridor (NE – SW)
- 3rd floor – room EL311 (S)
- 7th floor – room EK705 (W)

All windows and doors have aluminium frames with blue painted surface with thermal coefficient C_F = 2,2 $Wm^{-2}K^{-1}$. This energy non efficient solution has only architectonical and aesthetical background. The glazing consists from standard two layer insulating glass with coefficient C_G = 1,4 $Wm^{-2}K^{-1}$. All prospects are equipped with internal silver metal sunblindes [3].

Heavy building overheating resulting to very unpleasant labour conditions between late spring and early autumn became evident during the first operation years. Two projects were designed to solve this problem. The first one was based on installation of standard air conditioning, while the second one dealed with passive solar systems – namely external sunblindes. Lower purchase and operating costs evoked realization of the second project [3, 4].

External plastic sunblindes were installed on every window facing east, south and west. Design of the building requested blue coloured surface. Original miradors were accented to stand as basic solar windows. Building overheating was significantly decreased, but lighting conditions have got insufficient. Additional artificial lightning equipment seemed to be necessary although the sufficient illumination can be managed also with clever adjustment of segment inclination and retraction of particular sunblindes. Many users have reported decreased user comfort although the climate had became more comfortable. Issues with lighting have overrided proposed benefits. This effect tends unfortunately to only very limited usage of new installed system. System real efficiency is compared with original situation as described in the next paragraphs.

Practical and economical benefits of installed system are much lower than it was expected because of described reasons [3].

3. Building Surface Temperature Measurements

Characteristic sets of measuring points were defined and marked on the surface of all model rooms. Uneven emissivity of particular surface materials was matched with adhesive thin dull white paper foil. Sample configuration of measuring points in the model room on the 1st floor corridor (S) shows Fig. 2. This situation although demonstrates benefits of solar window.

Fig. 2. Configuration of measuring points in the 1st floor corridor (S).

Example of measured values in this location shows Table I. This exemplification demonstrates versatile conditions during late autumn or early spring season. Progress of temperatures [°C] for all measuring points is displayed for a sample day (22nd of November 2016) between effective sunrise 8:30 and sunset 16:10. Foolproof sun window caused measurable increase of internal walls temperature T_{wall} [°C].

Table I. – 1st floor corridor (S), 22.11.2016

22.11.		1	2	3	4	5	6	7	8
frame	8:30	13,4	10,7	13,6	11,9	21,2	20,4	23,5	24,2
	9:15	13,4	10,7	13,6	11,9	21,2	20,4	23,5	24,2
	10:00	15,8	13,5	16,4	15,1	22,6	22,3	24,7	25,2
	10:40	21,7	20,2	23,2	22,5	26,6	25,7	29,4	28,8
	11:20	26,4	25,5	28,6	27,8	29,9	29,1	32,0	32,5
	12:25	30,3	29,8	30,2	31,1	31,9	31,4	32,7	32,3
	13:10	31,7	33,1	31,5	32,3	32,4	31,9	24,8	23,0
	13:45	31,5	32,9	31,4	32,2	21,6	21,1	20,3	18,2
	14:30	27,4	26,1	24,2	27,8	17,9	17,3	18,6	16,3
	15:20	21,5	19,9	19,9	20,9	17,1	17,0	16,9	15,6
	16:10	17,1	15,1	17,6	16,3	14,6	14,8	14,9	15,1
22.11.		9	10	11	12	13	14		t_{wall}
glass	8:30	14,4	14,6	12,8	19,9	20,0	19,8		21,5
	9:15	15,6	15,9	14,2	21,0	21,1	21,0		21,7
	10:00	20,1	20,6	20,5	28,6	30,3	30,5		23,1
	10:40	29,4	29,1	30,1	34,9	36,4	37,3		23,7
	11:20	35,9	36,5	38,9	37,9	39,1	40,6		24,1
	12:25	36,9	36,8	39,1	38,0	38,8	39,7		23,9
	13:10	32,6	33,2	34,6	26,3	25,7	26,1		23,5
	13:45	24,5	24,4	26,0	22,1	21,9	21,5		22,8
	14:30	22,2	22,0	23,2	21,3	21,1	21,2		22,7
	15:20	21,0	20,8	21,9	21,0	20,3	20,4		22,5
	16:10	19,8	19,5	19,8	19,6	19,2	19,0		22,4

Fig. 3 presents temperature behaviour for different seasons to demonstrate particular benefits in the 1st floor corridor (S). The chart shows characteristic temperatures of frame and glazing surfaces (t_{frame}, t_{glass}).

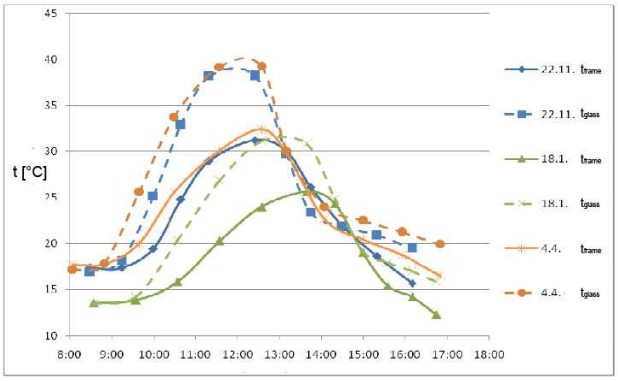

Fig. 3. Sample daily temperatures in the 1st floor corridor (S).

Characteristic temperatures for the 1st floor corridor (S) are calculated from the weighted average of particular measuring points on the frame (1) and glazing (2). The weight coefficients were set empirically.

$$t_{frame} = \frac{0{,}8t_1 + 0{,}6t_2 + t_3 + 0{,}9t_4 + t_5 + 0{,}9t_6 + 0{,}8t_7 + 0{,}6t_8}{8} \quad (1)$$

$$t_{glass} = \frac{0{,}8t_9 + 0{,}9t_{10} + 0{,}7t_{11} + 0{,}8t_{12} + 0{,}9t_{13} + 0{,}7t_{14}}{6} \quad (2)$$

Analogical equations with different number of elements (measuring points) and different weight coefficients (position) were used for all other model situations.

To avoid parasitic thermal flows and thermal persistence between sensors and the measured surfaces contact-less pyrometer Raytek Raynger ST was used for all these measurements.

Thermovision Fluke TiX640 and Flir T335 were used for visualization of temperature lay-out. Different construction materials with large range of emissivity complicate proper and accurate interpretation of recorded thermograms.

The emissivity depends not only on the chemical structure of the material, but also on surface treatment and color. This diversity cannot be eliminated sufficiently in this case [4].

Examples of measured thermograms are displayed on Fig. 4 and Fig. 5. Thermal gradient depending on the opening angle of particular sunblindes is evident on the frame in the middle of the picture and on the left side of the glazing on the Fig. 4. The effect on glazing on the right side is concealed under internal sunblindes.

These samples demonstrate passive solar system reducing surplus solar energy during hot season (3rd floor, room EL311 - S). Fig. 5 shows the same situation on the 5th floor (EL511 – S). The configuration of sunblinds is reverse to EL311. Vertical temperature dependency is evident between Fig. 4 and Fig. 5.

Fig .4. Sample thermogram (3rd floor, room EL311 - S).

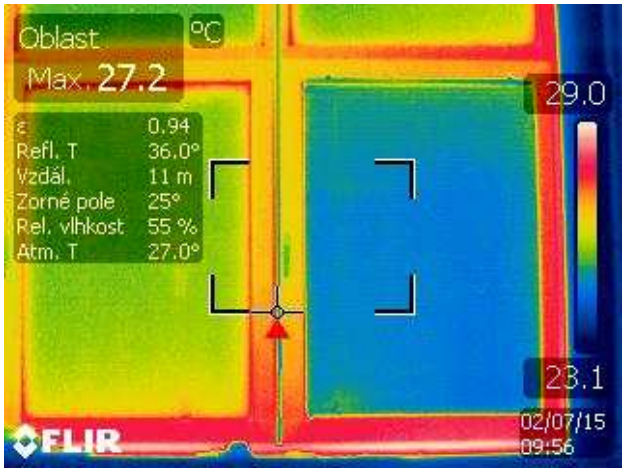

Fig .5. Sample thermogram (5rd floor, room EL511 - S).

Fig.6 demonstrates sample of reverse influence of passive solar system operating as additional isolation in cold season. Data were acquisited in the same location (EL311). External sunblindes are fully closed to eliminate looses of heat radiation and air circulation.

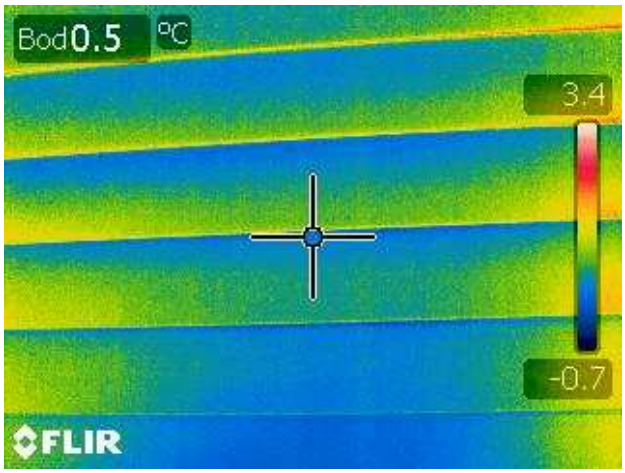

Fig .6. Detail thermogram (3rd floor, room EL311 - S).

The thermogram also visualises imperfect draught between particular segments accompanied with blows in the middle of the picture. Higher temperatures visible at the ends of all segments represent thermal sharing with surrounding non-isolated concrete construction.

Sample comparison between particular model locations during cold season is presented on Fig. 7. Fully pulled sunblindes in 1st floor corridor EU1 (S) caused faster but delayed temperature changes while the west facing window position affected the room EK703 (W) with delayed but lower value of maximum temperature.

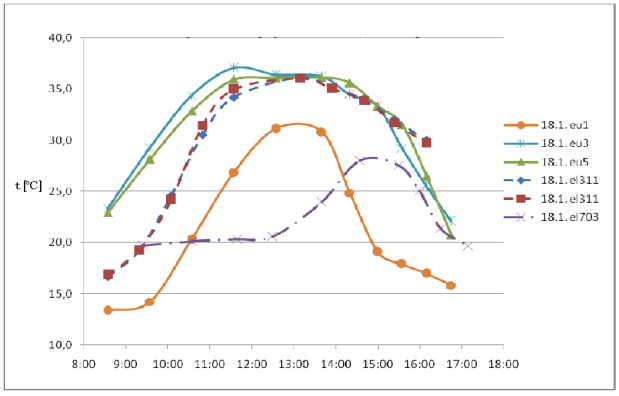

Fig .7. Sample glasing temperature (cold season).

Similar results for warm season are shown on Fig.8. Much faster temperature decrease in the 1st floor corridor EU1 (S) than similar decrees on Fig. 7 is the result of partial shading due to sunblindes construction. Also the sun in higher position in summer accents the results during colder months on Fig. 7.

Both figures also show influence of limited partial shading for situation EU3 and EU5 represented with 2 peaks along 11:00 – 14:00 and one dip around 12:00. Constructions of the sunblindes shade the sun in the highest position.

This typical effect of passive solar systems is more evident during the warmest months (may, june, july, august). Cases presented on Fig. 7 have this effect to be intentionally reduced to allow maximal energy gains requested during the cold season.

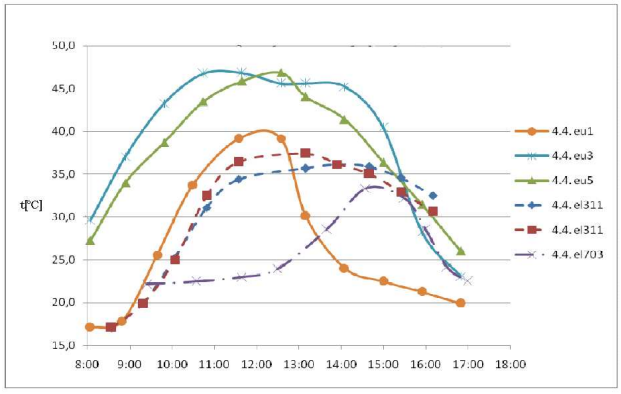

Fig .8. Sample glasing temeprature (warm season).

4. Calculations Of Penetrated Heat

Particular heat penetration through the windows Q_W (3) depends on insulated area, where A_F represents the surface of frames and A_G means surface of glazing. Q_S is value of local solar energy gain and S presents coefficient of shading [7].

$$Q_W = (A_F + A_G) \cdot \frac{A_G}{100 \cdot (A_F + A_G)} \cdot Q_S \cdot S \quad (3)$$

Fig. 9 illustrates the heat penetration through the window without any passive system (left side) and with primitive passive system (right side). Left window with retracted sunblindes is fully exposed to solar radiation, while a wet cotton curtain hanging over internal side of the window represents primitive passive solar system on the right.

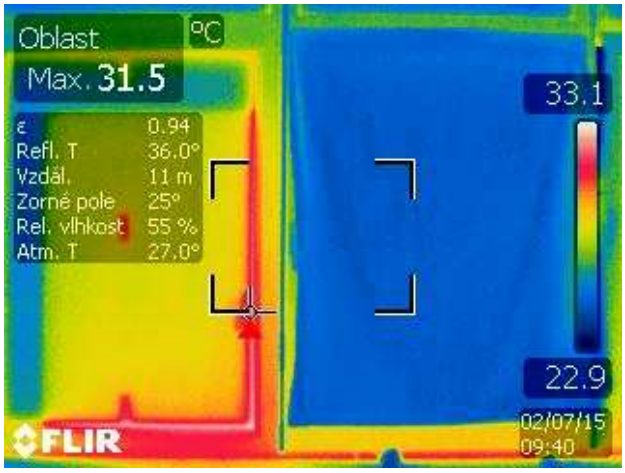

Fig .9. Sample glasing temeprature (warm season).

Fig. 11 demonstrates effect of local air circulation. Left side of the picture represents fully closed window while right part shows slightly open window with a slot at the top. Circulation of hot outside air is evident in the upper part of the window. Lower hot part of picture is the result of overheating due to air suction and chimney draught.

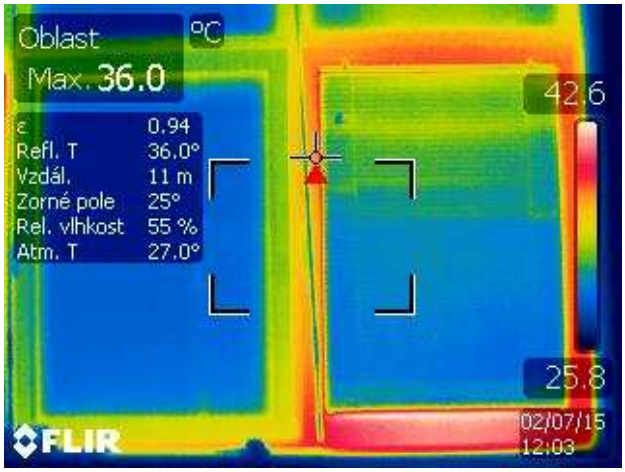

Fig .11. Effect of air circulation.

Local solar energy gain Q_S (4) can be integrated from the solar radiation intensity curve I between effective sunrise t_1 and sunset t_2 [8].

$$Q_S = \int_{t1}^{t2} I dt \quad (4)$$

Amount of relative heat penetration into or from a sample room q (5) depends on temperature of the inner surface t_1, exterior surface temperature t_2 and relative penetration constants α_1, α_2, λ, δ [7].

$$q = \frac{t_1 - t_2}{\frac{1}{\alpha_1} + \frac{1}{\alpha_2} + \frac{\delta}{\lambda}} \qquad (5)$$

Total energy gains and looses Q (6) are used either for technical or economical calculations and depend on internal temperature t_{IN}, window temperature t_W, surface S and total penetration constants α, β, λ.

$$Q = \alpha \cdot S \cdot (t_W - t_{IN}) + \beta \cdot \left(\frac{T_W}{100}\right)^4 + \gamma \cdot S \cdot (t_W - t_{IN}) \quad (6)$$

Fig. 10 demonstrates sample charts for solar radiation I used for calculations of solar energy gains. Values of intensity are continuously recorded using local weather station Davis Vantage Pro.

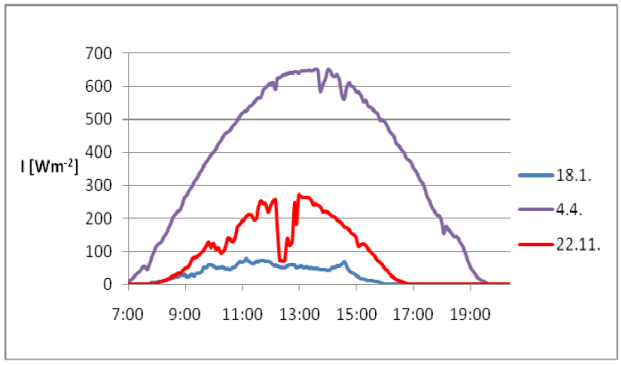

Fig .10. Solar radiation intensity.

Table II shows particular heat calculations for all 5 model rooms and for 3 sample measurements covering warm, cold and transient seasons. Total heat gain can be calculated as the sum of particular increments. Looses are indicated as negative values.

Table II. – Sample Energy Gain [Wm^{-2}]

	measurement	1	2	3	4	5
22.11.	8:30	22,51	17,98	22,85	19,99	35,62
	9:15	22,51	17,98	22,85	19,99	35,62
	10:00	26,54	22,68	27,55	25,37	37,97
	10:40	36,46	33,94	38,98	37,80	44,69
	11:20	44,35	42,84	48,05	46,70	50,23
	12:25	50,90	50,06	50,74	52,25	53,59
	13:10	53,26	55,61	52,92	54,26	54,43
	13:45	52,92	55,27	52,75	54,10	36,29
	14:30	46,03	43,85	40,66	46,70	30,07
	15:20	36,12	33,43	33,43	35,11	28,73
	16:10	28,73	25,37	29,57	27,38	24,53
18.1.	8:35	19,15	14,78	20,16	13,78	36,46
	9:35	24,02	19,66	26,54	21,17	39,31
	10:35	33,77	30,24	36,79	33,94	43,85
	11:35	41,50	40,82	47,38	46,37	50,06
	12:35	47,21	46,54	48,38	47,88	49,22
	13:40	54,77	52,92	46,54	45,70	34,10
	14:20	42,17	39,82	36,79	35,95	28,56
	15:00	31,92	29,90	31,58	30,24	26,38
4.4.	8:30	24,70	22,18	27,55	24,86	23,35
	9:15	23,86	21,50	27,38	24,36	22,51
	10:00	20,33	15,96	21,50	16,46	35,62
	10:40	24,86	20,83	26,54	22,85	38,14
	11:20	34,27	31,58	36,96	34,94	43,34
	12:25	41,83	41,50	46,70	45,53	49,06
	13:10	48,55	47,21	48,55	49,22	50,40
	13:45	54,77	54,10	50,06	48,72	45,70
	14:30	43,85	41,16	38,47	40,66	31,75
	15:20	34,61	30,91	32,59	32,42	27,72
	16:10	29,57	27,05	30,74	29,23	26,54

Presented table proves that reasonable amount of energy can be gained also during unpleasant conditions but using proper solar passive system. Positive energy gains during typical winter day (18.1) demonstrate this fact.

5. Results and Conclusions

These experiments have proven relevant influence of tested passive systems on the internal climate inside all sample rooms. The internal temperatures during warm season were for 4,1 – 6,3°C lower if compared to original situation. Also direct surface overheating of labour place was significantly eliminated, but this effect is not included in this paper.

System application during cold season increased the internal temperature for 1,3 – 3,4°C if compared to the original situation. Recalculation for entire building indicates heating costs savings during cold season for about 8%.

Economical benefits during warm season could not be calculated, because the building has no conventional air conditioning so the current cooling costs are zero. More favourable environment is positive for labour conditions and labour effectiveness.

Although the optimal operational regime of the passive system is much more complicated than in southern countries, usage of passive solar systems is still reasonable in central Europe. Balance between reduction of thermal gains and sufficient natural illumination requests sunblindes cyclic open / close operations.

While the internal temperatures are usually to be felt as more favourable, illumination demands are more complicated so the user comfort is often reported to be decreased. Further use of sophisticated controller instead of manually operated system would solve this issue, but purchase and operating cost are reasonably higher and can eliminate the economical benefits.

References

[1] ZOBAA, A., BANSAL, C. Handbook of renewable energy technology. Hackensack, N.J.: World Scientific, c2011.

[2] SØRENSEN, B., Renewable energy: physics, engineering, environmental impacts, economics & planning. 4th ed. Burlington, MA: Academic Press, c2011.

[3] HRBEK, J. Vliv pasivnich solarnich systemu na provoz budovy – Diploma thesis, ZCU, Plzen, 2017.

[4] FOKAIDES, P.A., KALOGIROU, S.A., Application of infrared thermography for the determination of the overall heat transfer coefficient (U-Value) in building envelopes. Appl Energy, 88, 2011.

[5] BALARAS, C.A., ARGIRIOU, A.A. Infrared thermography for building diagnostics Energy Build, 2002.

[6] LEHMANN, B., WAKILI, K.G., FRANK, T., COLLADO, B.V., TANNER, C. Effects of individual climatic parameters on the infrared thermography of buildings, Appl Energy, 2013.

[7] REHANEK, J., JANOUS, A., Tepelne ztraty budov a moznosti jejich zmensovani, SNTL, Praha, 1986.

[8] CIHELKA, J., Solarnitepelna technika, T.Malina, Praha, 1994.